Protein localization in electron micrographs using fluorescence nanoscopy

Shigeki Watanabe[1], Annedore Punge[2], Gunther Hollopeter[1], Katrin I. Willig[2], Robert John Hobson[1], M. Wayne Davis[1], Stefan W. Hell[2], and Erik M. Jorgensen[1*]

[1]Department of Biology and Howard Hughes Medical Institute, University of Utah, Salt Lake City, UT 84112-0840

[2]Department of NanoBiophotonics, Max Planck Institute for Biophysical Chemistry, 37077 Göttingen, Germany

* Corresponding author

Contact: jorgensen@biology.utah.edu

UU IR Author Manuscript

Abstract

A complete portrait of a cell requires a detailed description of its molecular topography: proteins must be linked to particular organelles. Immuno-electron microscopy can reveal locations of proteins with nanometer resolution but is limited by the quality of fixation, the paucity of antibodies, and the inaccessibility of the antigens. Here, we describe a method for correlative fluorescence electron microscopy (fEM) for the localization of proteins in electron micrographs. Proteins tagged with Citrine or tdEos were expressed in *Caenorhabditis elegans,* fixed and embedded. Tagged proteins were imaged from ultrathin sections using stimulated emission depletion microscopy (STED) or photoactivated localization microscopy (PALM). Fluorescence was correlated with organelles imaged in electron micrographs from the same sections. These methods were used to successfully localize histones, a mitochondrial protein, and a presynaptic dense projection protein in electron micrographs.

Background

Proteins can be imaged in cells by tagging them with fluorescent proteins or antibodies. However, the resolution of conventional optical approaches is limited to about 200 nm by the diffraction of light and to even poorer resolutions in practice[1]. By contrast, typical proteins are about 4 nm in diameter and may be associated with organelles as small as 30 nm. Thus, localization of proteins to cellular structures using fluorescence methods is fairly crude. Recently, fluorescence techniques capable of nanometer-scale resolutions ('nanoscopy')[2] have been developed. These methods overcome the diffraction limit by inhibiting fluorescence emission temporally so that fluorophores closer than the diffraction limit can be separated[2].

In stimulated emission depletion microscopy (STED)[3], fluorescence is inhibited by a beam of light, called the STED beam. Patterned as a doughnut and overlaid with the excitation beam of a scanning microscope, this beam ensures that only fluorophores in a narrow region around the doughnut center are allowed to fluoresce; the other molecules illuminated by the excitation light remain dark[4]. The image is obtained by scanning the beam across the sample, and is assembled from emissions defined by the position of the STED beam.

Photo-activated localization microscopy (PALM) and similar techniques (FPALM and STORM)[5-7] use molecules whose fluorescence is intrinsically inhibited; the absorption of a photon (usually ultraviolet) activates them as fluorophores. To separate features that are closer than the diffraction limit, only one fluorophore is randomly activated; the neighboring molecules remain dark. The position of the fluor is determined by calculating the centroid of the emission pattern. The registered molecules are subsequently turned off by bleaching, allowing adjacent molecules to be activated and become fluorescent. This sequence is continued until all molecules are registered. PALM differs from STED microscopy in that the coordinates of the fluorescence emission is calculated rather than defined by the beam of light[2].

Fluorescence nanoscopy can localize protein precisely[5], but the cellular context is limited in these images. Immunocytochemical electron microscopy (immuno-EM) can localize proteins to organelles. However, this method is compromised by technical difficulties including the destruction of antigens, inaccessibility of antigens, the lack of suitable antibodies, and nonspecific binding of antibodies[8-10]. Even when successful, the

UU IR Author Manuscript

size of antibodies (~19 nm in length)[11] limits the ultimate resolution that can be revealed, particularly when secondary antibodies are employed.

The advantage of fluorescence microscopy is that all proteins can potentially be tagged with a fluorophore. The advantage of electron microscopy lies in its exquisite depiction of subcellular structure. Since their strengths are complementary, these two methods could be very effective if combined[12,13]. PALM has been successfully performed on cryo-sectioned material fixed with aldehydes[5]. However, sub-cellular details are obscure in cryo-sections due to poor tissue contrast. Morphology could be improved using traditional EM techniques, but fluorescent proteins are quenched by the acidic, dehydrated and oxidizing conditions required for fixation and polymer embedding of the specimen[14].Ultimately, a compromise must be found between preservation of fluorescence and morphology.

Here we describe a method that uses both STED and PALM on ultrathin sections of fixed tissues to localize proteins at the nanoscale and subsequently correlate protein localization with ultrastructural features revealed by electron microscopy.

Results

Development of the method

To develop a practical method for correlative fluorescence electron microscopy, we optimized each step of sample preparation, balancing the requirements for fluorescence and ultrastructure. We used the nematode *Caenorhabditis elegans* as our model system because fluorescently tagged proteins can be stably expressed[15,16] and methods for electron microscopy are well-established[9].

Choice of target proteins

To evaluate fluorescence localization in electron micrographs, proteins with well-described localizations were tagged. We chose three proteins to test our method: Histone, TOM-20, and Liprin. Histones (HIS-11) are localized to the nucleus. The nucleus can be easily visualized using a conventional light microscope, and thus is ideal for rapid optimization of preservation of fluorescence. TOM-20 (translocase of outer mitochondrial membrane-20) is a 20kDa outer membrane protein of mitochondria. A cross-section of mitochondria can be as narrow as 150 nm in diameter, which is below the diffraction limit, and thus TOM-20 localization is a good test of super-resolution methodologies. α-liprin (SYD-2) is localized to the presynaptic dense projection[17]. Neurons in *C. elegans* are the most sensitive tissue to the fixation conditions, and Liprin localization required us to fully optimize our protocol.

Optimization of fixatives

Fixatives crosslink cellular structures and protect the tissue from distortions caused by dehydration and embedding in plastic. Aldehyde-based fixatives, especially glutaraldehyde, crosslink proteins very effectively. Metallic oxide fixatives, such as osmium tetroxide, crosslink unsaturated lipids in membranes[18]. Since osmium tetroxide scatters electrons, it also acts as a contrast enhancer for membranes. These fixatives also have disadvantages for fluorescence microscopy. Glutaraldehyde induces autofluorescence in fixed tissues[19]. Osmium tetroxide is a very strong oxidizing agent and can break peptide bonds –GFP fluorescence is quenched by oxidation[14]. Thus, we tested

multiple combinations of fixatives at varying concentrations to balance the preservation of morphology and fluorescence.

To evaluate the preservation of both fluorescence and morphology, we processed transgenic animals expressing Citrine or tdEos fused to histone H2B. For each treatment, animals were evaluated on a compound microscope prior to polymerization of the plastic to gauge the amount of fluorescence loss due to the fixation. Morphology was evaluated from ultra-thin sections of neurons since the neurons are the most sensitive tissue to fixation conditions. As anticipated, fixation with aldehyde-based fixatives (paraformaldehyde, glutaraldehyde, and acrolein) resulted in the induction of autofluorescence. Autofluorescence could be quenched by 1% sodium borohydride[19], but cell membranes were not well-preserved by aldehyde-based fixatives (**Supplementary Fig. 1a,b**). A low concentration of osmium tetroxide (0.1%) preserved membrane morphology effectively, but fluorescence was reduced to less than 10% after fixation and plastic embedding (**Supplementary Fig. 1c,d**). If osmium tetroxide was applied at concentrations of less than 0.1%, significant degradation in the tissue morphology was observed. An alternative lipid cross-linking agent, potassium permanganate[9] preserved membrane morphology well. Despite the fact that potassium permanganate is also an oxidizing agent, the fluorescence was about 30-fold brighter than with 0.1% osmium tetroxide (**Supplementary Fig. 1f**). However, synaptic vesicles appeared to be missing from the synaptic terminals (**Supplementary Fig. 1e**). To further optimize membrane morphology, 0.001% osmium tetroxide was added to 0.1% potassium permanganate. With this cocktail, the morphology of neurons was better than either fixative alone at these concentrations (**Supplementary Fig. 1g**). Fluorescence was almost as bright as with 0.1% potassium permanganate alone, that is, fluorescence levels were 40% of untreated animals (**Supplementary Fig. 1h**), and strong fluorescence was observed for both Citrine and tdEos after sectioning (**Fig. 1a,e**).

Optimization of plastic

Following fixation, tissue samples were embedded in plastic resin for ultrathin sectioning. Polymerization typically requires dehydration and heat, which tend to denature proteins, including fluorophores. We tested the following four hydrophilic resins capable of low temperature polymerization: Lowicryl K4M, LR Gold, LR White, and glycol methacrylate (GMA). Animals expressing Citrine or tdEos fused to histone (P*hsp-16.41::fluor::his-11::unc-54 3'UTR*) were processed as described in the previous section and embedded in either K4M, LR Gold, LR White, or GMA. Additionally, water (2-5%) was included in each resin. Fluorescence preservation and sectioning quality were assessed after polymerization.

K4M, the most hydrophilic resin, is reportedly capable of tolerating up to 10% water by weight[20]. However, in our hands, inclusion of 5% water reduced the sectioning quality of the tissues beyond an acceptable level due to poor polymerization.

LR Gold and LR White are very similar in their formula and chemistry; however, slightly different problems arose with polymerization. LR Gold polymerized rapidly but did not penetrate the tissue. The pH of LR White was too acidic for most fluorescent proteins; the pH with 2-5% water was quite low (~5.5). Neutralizing the pH of the plastic using ethanolamine preserved fluorescence (**Supplementary Fig. 1**) and resulted in good

morphology (**Supplementary Fig. 1g**, **Fig. 2g**). However, batch-to-batch variability in pH and water capacity of LR White resulted in irregular polymerization.

GMA, by contrast, *requires* 3% water for polymerization at pH8, fulfilling both the hydration and alkalinity requirements of the fluorophores. Fluorescence was slightly brighter in GMA embedded samples compared to LR White. Moreover, application of water to ultra-thin sections collected from animals embedded in GMA immediately increased fluorescence intensity by 30%. This restoration of fluorescence suggests that a large fraction of the fluorescent proteins are maintained in a non-fluorescent, dehydrated state and that about 70% of the fluorescence observed before fixation can be preserved. Ultrathin sections were difficult to cut because GMA does not cross-link to the cuticle like epoxy resin, and thus the tissue usually breaks loose from the surrounding resin if sectioned below 70 nm. However, ultrastructure could be resolved even on thicker sections by using low accelerating voltage and collecting back-scattered electrons on the scanning electron microscope (**Fig. 2c**, for example).

Correlative fluorescence nanoscopy and electron microscopy

Proteins tagged with Citrine were imaged using STED microscopy (**Fig. 1a,b**, **Fig. 2 a,b**, **Fig. 3a,b**). Transgenic strains expressing Citrine-tagged proteins were embedded in GMA and sections cut at approximately 100 nm thick to ensure a sufficient signal strength. In confocal mode, fluorescence was diffuse, but resolution was greatly improved by applying STED. Resolution of STED fluorescence in these images was determined to be 60-80 nm by Full-Width Half-Maximum (FWHM) analysis of point-like emitters. It is difficult to assign histone fluorescence to a particular structure within the nucleus (**Fig. 1b**) but it is clearly restricted to profiles within the shape of a nucleus. STED images of tagged-TOM-20 are resolved into circular rings (**Fig. 2b**). A single fluorescent spot in the confocal image of tagged Liprin, resolves into a smaller circle in the STED image but does not form a recognizable structure as expected for this very small organelle (**Fig. 3b**). Corresponding scanning electron micrographs were acquired from the same sections used for STED imaging. The STED images were then aligned to the electron micrographs using fluorescent silica beads as fiduciary marks, which were applied onto the sections prior to fluorescence imaging. The beads are fluorescent in the UV (excitation 354 nm, emission 450 nm) and detected by an additional imaging scan after recording the STED data. Silica beads become charged and reflect the electrons, which results in black circles of 1 μm in electron micrographs. The organization of labeled histones into chromatin aligns on top of the profile of a nucleus (**Fig. 1c,d**). The rings of TOM-20-Citrine seen in the STED image align with the outer membranes of mitochondria (**Fig. 2c,d**). The liprin-Citrine spots observed in the STED images localize to a presynaptic dense projection observed in electron micrographs (**Fig. 3c,d**).

For PALM, the target proteins were fused to tdEos or Dendra and transgenic animals were fixed under the same conditions. Resolution in PALM depends on the number of photons collected from each fluorescent protein, and the localization precision is determined as a function of molecular photon statistics, background noise, and pixilation[21]. Given the signal-to-noise ratio achieved by Dendra and tdEos, we were able to calculate a localization precision of 12 nm (see Methods). Section thicknesses for PALM were about two thirds of those used for STED and the fluorescent signals were correspondingly reduced compared to STED. Fluorescence localization was as expected:

Histone fluorescence corresponded to the size of the nucleus and appeared as circles several micrometers in diameter (**Fig. 1f**). TOM-20 signals were confined to rings, but were considerably less intense than those observed in the STED image (**Fig. 2f**). Liprin signals were rare and uninterpretable in the absence of ultrastructural information (**Fig. 3f**). PALM fluorescence was correlated to the electron micrographs using 100 nm gold nanoparticles for fiduciary markers (**Supplementary Fig. 4**). Gold nanoparticles are fluorescent[22]: particles were excited with a 561 nm laser and emission collected at 580 nm to mark the fluorescence micrographs. Gold particles also reflect the electron beam in the scanning electron microscope and mark the micrograph. In the alignments, tagged histones were localized within the nucleus but not the nucleolus (**Fig. 1 g,h**). The distribution of histones in the nucleus seems to differ from the distribution observed using STED, but these differences are likely due to the cell type rather than the technique (**Supplementary Fig. 5**). TOM-20 molecules were localized to the outer membrane of mitochondria (**Fig. 2 g,h**). Tagged liprin was expressed from multi-copy arrays for both STED and PALM imaging. Overexpression resulted in aggregations of the protein in the cell body adjacent to the nucleus (visible in the upper left corner of **Fig. 3h**, **Supplementary Fig. 2**). Liprin signals at the synapse were precisely localized to the presynaptic dense projection (**Fig. 3 g,h**).

Discussion

Fluorescence nanoscopy allows one to precisely pinpoint the location of a single molecule in a cell[3,5]. However, precise localization in a field of black is not useful. Where is that protein in the context of cellular structure? Where are previously described organelles in relationship to this protein? Here, we demonstrated that fluorescently tagged proteins can be correlated with ultrastructure in electron micrographs to identify the cellular location of a protein. Four issues bear discussion: scanning electron microscopy, fluorescence sensitivity, fluorescence resolution, and nanoscopic methodology.

For correlative fEM (fluorescence electron microscopy), scanning electron microscopy offers several advantages over transmission electron microscopy because of the mounting surface and section thickness. First, sections for scanning electron microscopy can be mounted on a coverglass. This allows hundreds of sections in long ribbons to be examined for fluorescence, which can later be assembled for array tomography[13]. Moreover, PALM imaging is performed in the TIRF configuration, which requires mounting on a coverglass. Second, thick sections can be imaged with high resolution in scanning but not transmission electron microscopy. Sections must be relatively thick (70-100 nm) for two reasons: sections must be deep enough to produce an adequate fluorescent signal, and it is difficult to cut acrylic resins thinner than 70 nm. Although thick sections obscure ultrastructure in transmission electron microscopy, in scanning electron microscopy, low accelerating voltages can be used so that only the top 30 nm reflects electrons[23].

On the other hand, the images from the scanning electron microscope are not as crisp as those from a transmission electron microscope. Blurriness arises from two drawbacks of fEM imaging: beam diameter and stains. Transmission electron microscopes can achieve a resolution of less than 1 nm. However, the beam diameter for a scanning electron microscope is 4.5 nm when it is operated at 5 keV[23]. Second, the production of back-scattered electrons requires stains with high atomic numbers such as

osmium and uranium, but such staining quenches fluorescence and could not be used in our protocols before fluorescence imaging. Post-staining with uranyl acetate after fluorescence imaging helps significantly but still does not produce crisp images of internal membranes such as the lipid bilayers of synaptic vesicles. One potential solution would be to apply electron tomography which might compensate for the poor staining.

Correlative fEM represents an improvement of sensitivity over immunoEM. In many cases antibodies that work on plastic sections are not available. Although antibodies can penetrate somewhat into resins such as LR White, access to antigens remains limited in immunoEM[5]. Since correlative fEM does not rely on immunocytochemistry, antibody availability is not a concern, and fluorescent proteins deep within the plastic section can be localized. On the other hand, not all proteins tolerate tags with fluorescent proteins. In this case, if antibodies are available, they can be used for nanoscopic imaging of sections and could even be adapted for array tomography[11]. Despite the sensitivity of fEM, at this point the method is not quantitative. Under our conditions about 30% of the fluorescence is lost due to the oxidizing fixatives required for membrane preservation. Truly quantitative methods await the development of more robust fluorescent proteins.

The resolution of a conventional fluorescence microscope is limited to 200 nm. In practice multiple fluorescence sources scatter the signal at high magnification into a large and blurry blob. Under optimal conditions, STED or PALM resolve a fluorescent source to 30 or 20 nm[3,5], respectively. At these resolutions we can localize proteins to substructures of organelles in two dimensions. fEM can also achieve higher axial resolution than current methods in nanoscopy. Z-axis resolution in fluorescence microscopy is 700 nm, 2-3 times worse than in the X-Y axes[24]. Axial resolution can be improved by using two objective lens in the 4Pi microscope[23], isoSTED[25], and iPALM[26], but these arrangements have their own limitations. By sectioning the tissue into 70 nm serial sections, subdiffraction resolution is imposed on the signal simply by section thickness. Superresolution in three dimensions can be achieved by reconstructing the volume of the tissue[13,27].

The two methodologies used here, STED and PALM, each offer advantages and disadvantages relative to sensitivity and resolution, and a choice must be made depending on the application. STED is robust because Citrine is bright, and this fluorophore survives sample preparation well. STED is preferable if protein levels are low and as a consequence the signal is highly sensitive to oxidation. We observed that PALM generates weaker signals due to sensitivity of the photoconvertible fluorophoress to oxidation and higher background fluorescence than STED. The background signals in PALM however can be reduced by pre-bleaching the sample with intensive 561 nm laser and imposing a threshold for emission period. PALM provided high-resolution fluorescence signals and will be arguably more useful when imaging small and crowded structures like those within the synapse.

In conclusion, correlative subdiffraction-limit fluorescence microscopy and electron microscopy add a new method to protein localization. This method can potentially reveal the ultrastructural localization of proteins with greater resolution, sensitivity and fidelity than previously possible.

Acknowledgements

We thank Harald Hess and Eric Betzig (Janelia Farm) for access to the PALM microscope for proof-of-principle experiments, Richard Fetter (Janelia Farm) for sharing protocols, reagents and encouragement. We thank Michael Davidson (Florida State), Geraldine Seydoux (Johns Hopkins), Stefan Eimer (European Neuroscience Institute), Rudolf Leube (Universität Aachen), Keith Nehrke (University of Rochester), Christian Frøkjær-Jensen (Utah), Aude Ada-Nguema (Utah) and Marc Hammarlund (Yale) for DNA constructs. We thank Marine Biological Laboratory for equipments and funding for pilot experiments. We also thank Carl Zeiss Inc. for providing access to a beta version of the PAL-M.

Author contributions

S.W. and E.M.J. conceived and designed experiments. G.H., R.J.H. and M.W.D. provided strains and advice. S.W. optimized the methods, prepared the samples, performed PALM imaging. A.P. and K.I.W. performed STED imaging. S.W., S.W.H., and E.M.J. wrote the manuscript. S.W.H. and E.M.J. provided funding (NIH, NS034307; NSF, 0920069; MBL, DART fellowship). E.M.J. is an investigator of Howard Hughes Medical Institute.

Figure legends

Figure 1: Correlative fluorescence and electron microscopy using Histone fusion proteins. (**a**) Confocal image of Histone-Citrine acquired from a thin section (120 nm). (**b**) Corresponding STED image of Histone-Citrine. (**c**) Electron micrograph of an intestinal cell nucleus acquired from the same section. (**d**) Correlative STED and electron microscopy of Histone-Citrine. The fluorescent signals are tightly localized to the nucleus. (**e**) Sum TIRF image of Histone-tdEos acquired from a thin section (70 nm). Sum TIRF image represents all the photons detected by the camera during the experimental time course. (**f**) Corresponding PALM image of Histone-tdEos. (**g**) Electron micrograph of a muscle cell nucleus acquired from the same section. (**h**) Correlative PALM and electron microscopy of Histone-tdEos. The fluorescent signals are tightly localized to the nucleus. Scale bars, 3 μm (**a**-**d**) and 1 μm (**e**-**h**).

Figure 2: Correlative fluorescence and electron microscopy using TOM-20 fusion proteins. (**a**) Confocal image of TOM-20-Citrine acquired from a thin section (120 nm). (**b**) Corresponding STED image of TOM-20-Citrine. (**c**) Electron micrograph of a body wall muscle acquired from the same section. Note that at 120 nm the sections are relatively thick, but high resolution images can be obtained using a scanning electron microscope. (**d**) Correlative STED and electron micrographs of TOM-20-Citrine. The fluorescent signals are localized to the outer membrane of the mitochondria. (**e**) Sum TIRF image of TOM-20-tdEos acquired from a thin section (70 nm) of an LR White-embedded sample. (**f**) Corresponding PALM image of TOM-20-tdEos. (**g**) Electron micrograph of a body wall muscle acquired from the same section. (**h**) Correlative PALM and electron microscopy of TOM-20-tdEos. The fluorescent signals are localized to the outer membrane of the mitochondria. Note that PALM images of TOM-20-tdEos are from tissue embedded in LR White; all other samples are in GMA. Scale bars, 1 μm (**a**-**d**) and 2 μm (**e**-**h**).

Figure 3: Correlative fluorescence and electron microscopy using liprin fusion proteins. (**a**) Confocal image of Liprin-Citrine acquired from a thin section (70 nm). (**b**) Corresponding STED image of Liprin-Citrine. (**c**) Electron micrograph of neurons in the nerve ring acquired from the same section. (**d**) Correlative STED and electron microscopy of Liprin-Citrine. The fluorescent signals are localized to the presynaptic dense projection. (**e**) Sum TIRF image of Liprin-Dendra acquired from a thin section (70 nm). * represents a region of predominant background signal, which was discarded by emission time threshold. (**f**) Corresponding PALM image of Liprin-Dendra. (**g**) Electron micrograph of neurons from the head ganglion region acquired from the same section. (**h**) Correlative PALM and electron microscopy of Liprin-Dendra. The fluorescent signals are localized to the presynaptic dense projection. Aggregrations of the overexpressed liprin also appears in the cell bodies. 'mito', mitochondrion.; 'SV', synaptic vesicle. Scale bars, 500 nm (**a**-**h**).

Methods

Strains

Strains are listed in the **Supplementary Note 1**.

Oligonucleotides

Oligonucleotides are listed in the **Supplementary Table 1**.

Fluorescent labels of organelles

For Histone, a minigene encoding Citrine with worm-optimized codons and three artificial introns (Stefan Eimer) was amplified by PCR using the primers oGH55 and oMPD6. This amplification introduced flanking *att*B recombination sites and the resulting product was recombined with pDONR 221 (Invitrogen) using BP Clonase II (Invitrogen) to produce the *att*L1/*att*L2-containing entry clone [1-2]*Citrine* (pGH114). A similar strategy with primers oGH95 and EOS_rev was used to clone *tdEos* (Michael Davidson), resulting in [1-2]*tdEos* (pGH270).

The open reading frame (ORF) of a worm histone (*his-11*) was released from the plasmid *Ppie-1::GFP::HIS-11::pie-1 3'UTR* (pJH4.52, Geraldine Seydoux) by restriction digest with SpeI and ligated into the multiple cloning site in front of the *unc-54 3'UTR* in pMH472 (Marc Hammarlund). The resulting *att*R2/*att*L3-containing entry clone (pGH42) translationally fuses a histone onto the carboxy-terminus of ORFs of fluorescent proteins in [1-2] entry clones when recombined in a Multisite Gateway LR reaction (Invitrogen). The heatshock promoter (P*hsp-16.41*) in an *att*L4/*att*R1-containing entry clone (pCM1.57, Geraldine Seydoux) was used to drive expression of the fluorescent histones in an inducible manner. To enable directed insertion of the transgenes into the *C. elegans* genome, the recombination reactions were performed using the *att*R4/*att*R3-containing destination vector (pCFJ150, Christian Frøkjær-Jensen) that includes genomic fragments flanking a *Mos1* transposon insertion (*ttTi5605* II) for targeting, along with the *unc-119* gene from *C. briggsae* for selection. Recombination of pCM1.57, pGH114, pGH42 and pCFJ150 using LR Clonase II Plus (Invitrogen) generated P*hsp-16.41::Citrine::HIS-11::unc-54 3'UTR* (pGH201), while recombination of pCM1.57, pGH270, pGH42 and pCFJ150 generated P*hsp-16.41::tdEos::HIS-11::unc-54 3'UTR* (pGH154).

The expression constructs were integrated using *Mos1*-mediated single copy insertion (MosSCI) as described previously[16]. Briefly, *unc-119(ed3)* III mutants containing *ttTi5605* II (EG4322) were injected with a mixture of plasmids containing the *Mos1* transposase to mobilize the transposon, the targeting vector to provide a repair template for the resulting chromosomal break, and red fluorescent markers expressed in muscles and neurons to mark extrachromosomal arrays. Offspring of the injected animals were selected 2-4 generations later for homozygous *unc-119* rescue and the appearance of fluorescent nuclei following heatshock. MosSCI of pGH201 generated the strain EG5582 *oxSi282*[P*hsp-16.41::Citrine::his-11::unc-54 3'UTR*] II ; *unc-119(ed3)* III, and MosSCI of pGH154 generated the strain EG5576 *oxSi283*[P*hsp-16.41::tdEos::his-11::unc-54 3'UTR*] II ; *unc-119(ed3)* III.

For TOM20, to generate [2-3] entry clones that would fuse fluorescent tags onto the C-terminus of proteins encoded by [1-2] entry vectors, Citrine was amplified with oGH76 and oGH57, while tdEos was amplified with oGH96 and oGH94. These PCR products were each inserted between the *att*R2 and *let-858 3'UTR* of pADA-126 (Aude Ada-Nguema) by amplifying this [2-3] entry vector with oGH38 and oGH39 and using In-Fusion PCR Cloning (Clontech) to produce [2-3]*Citrine::let-858 3'UTR* (pGH113) and [2-3]*tdEos::let-858 3'UTR* (pGH271).

The first 54 amino acids of the TOM-20 subunit (F23H12.2) of the outer mitochondrial membrane translocase was BP cloned to produce the [1-2] entry clone pMH496 (Marc Hammarlund). This protein sequence is sufficient for protein targeting to the outer membrane of mitochodria[28]. The *myo-3* promoter in a [4-1] entry vector was from Open Biosystems (p_K12F2.1_93). LR recombination of [4-1]P*myo-3*, pMH496, pGH113 and the destination vector pDEST R4-R3 (Invitrogen) generated P*myo-3::TOM-20(N-term)::Citrine::let-858 3'UTR* (pGH194), while recombination of [4-1]P*myo-3*, pMH496, pGH271, and pCFJ150 produced P*myo-3::TOM-20(N-term)::tdEos::let-858 3'UTR* (pGH158).

EG5515 *lin-15(n765ts)* X ; *oxEx1329* [P*myo-3::TOM-20(N-term)::Citrine::let-858 3'UTR lin-15(+)* LITMUS 38i] was made by injecting MT1642 *lin-15(n765ts)* with 33 ng/ul each of pGH194, *lin-15* rescuing plasmid pL15EK[29], and LITMUS 38i (NEB). MosSCI of pGH158 resulted in EG5998 *oxSi203* [P*myo-3::TOM-20(N-term)::tdEos::let-858 3'UTR unc-119(+)*] II ; *unc-119(ed3)* III.

To tag SYD-2, the α-liprin (*syd-2*) gene was amplified with oRJH19 and oRJH20 from genomic DNA. The resulting PCR product was BP cloned into pDONR 221 (Invitrogen) to generate [1-2]*syd-2* (pRH247, Robert Hobson). To generate [2-3] entry clones that would fuse fluorescent tags onto the C-terminus of proteins encoded by [1-2] entry vectors, pDendra2 was amplified from *Prab-3::TBA-1::Dendra2::unc-54 3' UTR* (pWD264) with oRJH21 and oRJH22. This PCR product was then cloned into pGH38 as BamHI-SpeI fragment. To drive expression in the nervous system, the promoter of *snt-1* was amplified with oRJH23 and oRJH24 from genomic DNA. The resulting PCR product was BP cloned into pDONR P4-P1R (Invitrogen) to produce [4-1]P*snt-1* (pCFJ284, Christian Frøkjær-Jensen). LR recombination of pCFJ284 pRH247 and pCFJ150 with either pGH113 or pWD240 resulted in P*snt-1::SYD-2::Citrine::let-858 3'UTR* (pRH409) and P*snt-1::SYD-2::Dendra2::let-858 3'UTR* (pRH419).

EG6190 *ttTi5605; unc-119; oxEx1490*[P*snt-1::SYD-2::citrine*; *unc-119(+) lin-15(+)*] was made by injecting EG4322 *ttTi5605; unc-119(ed3)* with 25 ng/ul of pRH409 and 75ng/ul pL15EK. EG6191 *ttTi4348; unc-119; oxEx1491*[P*snt-1*::*SYD-2::Dendra2*; *unc-119(+) lin-15(+)*] was made by injecting EG5299 *ttTi4348; unc-119(ed3)* with 25 ng/ul of pRH409 and 75ng/ul pL15EK. All constructs were designed using APE. (http://www.biology.utah.edu/jorgensen/wayned/ape/)

Choice of fluorescent proteins

Fluorescent proteins, Citrine for STED and PALM for tdEos or Dendra, were chosen based on their characteristics and expressions in *C. elegans* (see **Supplementary Note 2** for details).

Sample preparations for correlative microscopy

The sample preparation for electron microscopy consists of six steps: rapid freezing, acetone substitution, fixation, staining, infiltrating with plastic, and polymerizing the plastic (see **Supplementary Note 3** for details).

High-pressure freezing and freeze-substitution

The fixatives and freeze-substitution media, 95% anhydrous acetone (EMS, RT10016) and 5% water were mixed in the cryogenic vials (Nalgene, #5000-0020) (see **Supplementary Note 4** for use of 5% water) and frozen in liquid nitrogen prior to use. Acetone was used as the organic solvent in all fixations. In contrast with acetone, ethanol extracted membranes from neuronal tissues. This result was consistent with the idea that acetone acts as a fixative during the freeze-substitution[30].

The fixatives used here are 0.1-2% paraformaldehyde (EMS, #RT15710), 0.1%-1% glutaraldehyde (EMS, #16530), a combination of paraformaldehyde and glutaraldehyde, 0.1% acrolein (Sigma-Aldrich, #01680-250ML), 0.001%-0.5% osmium tetroxide (EMS, RT19134) , 0.1% potassium permanganate (EMS, RT20200), and a combination of osmium tetroxide and potassium permanganate.

Animals expressing fluorescently tagged proteins were placed onto a 100 μm deep, type-A specimen carrier, filled with bacteria (OP50 or HB101) and were instantaneously frozen in a BAL-TEC HPM 010 high pressure freezer (BAL-TEC, Liechtenstein). The specimens were transferred into a cryogenic vial containing freeze-substitution media and fixatives. The cryogenic vials are then transferred into an automatic freeze substitution unit (Leica Microsystems, AFS 2), and the specimen was freeze-substituted with the following program: 30 hours at -90ºC, 5ºC/hour to -20ºC, and 2 hours at -20ºC.

Infiltration

Acetone and fixatives were completely washed out from tissues using 95% ethanol prior to infiltration because the residual acetone causes improper polymerization due to its action as a free radical scavenger. Infiltration (30% for 5 hours, 70% for 6 hours, and 95~98% for overnight) was carried out at -20ºC in cryogenic vials. After the removal of fixatives, the specimens were washed with 95% ethanol over 2 hours. Ethanol was prepared by adding 5% milliQ water to anhydrous ethanol (Sigma-Aldrich, #459844-

1L). The solutions for infiltration were prepared by mixing 100% stock plastic solutions with 95% ethanol in glass scintillation vials (EMS, #72632). Mixing the solutions in plastic vials will cause incomplete polymerization. The formulas for 100% stock solutions are as follows. We have tested following four resins: Lowicryl K4M (EMS, #14330), LR Gold (EMS, #14370), LR White (EMS, #14381-UC), and glycol methacrylate (GMA, SPI Supplies/Structure Probe, Inc., #02630-AA). The components for these resins are listed in the **Supplementary Note 5**. For K4M, 17.3 g methacrylic and acrylic esters, 2.7 g triethyleneglycol-di-methacrylate, 10 g benzoin-methyl-ether, and 5% water were mixed. LR Gold was mixed with 5% water. 10 g of catalyst, benzoyl peroxide, was mixed in 500 ml LR White one day prior to use. pH of LR White with 2-5% water tended to be low (~5.5), which was too acidic for most fluorescent proteins. Therefore, we neutralized the pH using ethanolamine as follows. The catalyzed LR White was mixed with 2-5% water depending on the batch and neutralized with ethanolamine (5 µl in 20 ml of catalyzed LR White). We found that fully neutralized LR White (pH 7-7.4) could not be completely polymerized, and the sections were torn or destroyed upon sectioning. We determined the amount of ethanolamine compatible with full polymerization to be 0.025% (5 µl in 20 ml of LR White), which increased the pH to 6.5. The pH of the catalyzed LR White drops significantly as the storage period increases, and thus we only used catalyzed LR White that was less than one month old. For GMA, 67 ml glycol methacrylate, 30 ml butyl methacrylate, 3 ml water, and 0.6 g benzoyl peroxide were mixed and used for all infiltration steps.

Polymerization

The animals are dissociated from bacteria, which was the space-filler for high pressure freezing. Since acrylic resins do not cross-link to tissues, in particular the cuticle, the tissues needs to be surrounded by the plastic as much as possible. Otherwise the tissue can break away from the matrix and experience distortion. The animals are then embedded in a cap of a polypropylene BEEM capsule (EBSciences, #TC). Polypropylene capsules were used since LR White does not polymerize completely in a polyethylene capsule. A disc of aclar film (EMS, #50425-10) was placed in the bottom of the BEEM capsule, prepared by 3/8" DISC Punches (Ted Pella Inc., #54741). A few animals from each condition were mounted on the glass slide prior to polymerization, and the fluorescence was observed on a Zeiss Axioskop with a 63x plan-Apochromat (NA=1.40) objective and imaged using a digital camera (Diagnostic Instruments, Inc., #25.1). ImageJ was used to measure the photon intensity in each case.

For K4M and GMA polymerization, 1 ml of K4M or GMA was mixed with 1.5 µl N,N-Dimethyl-p-toluidine (Sigma-Aldrich, #D9912) and dispensed into the embedding cap containing the specimen. For LR Gold polymerization, 0.1% benzoyl peroxide was mixed into LR Gold, and the catalyzed LR Gold was applied to the specimens in the embedding cap. For LR White polymerization, LR White accelerator (Ted Pella Inc., #18185) was added at 1.5 µl per 1 ml of the catalyzed LR White. The embedded specimens are filled with this mixture. In each case, the embedding caps were covered with another layer of aclar film in order to block oxygen and thus allow polymerization of the plastic. The polymerization was carried out over 24 hours. The polymerized blocks are stored in nitrogen-filled, vacuumed bags in the freezer at -20ºC if not sectioned immediately. 70-500 nm sections were collected on coverslips using an

ultramicrotome (Leica microscystems, UC6) and imaged using a Zeiss Axioskop. For STED and PALM imaging, 70-100 nm ultra-thin sections were collected from each strain mounted on the pre-cleaned coverslips (#1.5, 18mm x 18mm for STED and #1.5, 25 mm diameter for PALM).

Fluorescence quantitation

Loss of fluorescence intensity was monitored using ImageJ through all procedures from post-infiltration to sections. Using a point selection tool, the intensity of 3-4 fluorescent spots from 2-3 animals in each condition was measured. The obtained values were averaged and compared.

Coverslip cleaning

Coverslips for PALM imaging were incubated in the Piranha solution (3 parts sulfuric acid: 1 part hydrogen peroxide) for an hour to reduce background fluorescence. The Piranha solution was then washed off thoroughly six times with milliQ water. The coverslips were then sonicated for half an hour. The water was washed off again for 6 times. The coverslips were dipped into 100% methanol to make the surface hydrophobic, which allows easy pick-up of sections. The coverslips were then air-dried.

Storage and shipment of specimens

Although fluorophores can be preserved effectively through electron microscopy preparation, we found the fluorescence to be very sensitive to storage conditions, specifically ambient air and temperature. Fluorescence is quenched if the samples are left out in the air at room temperature for a few days. We found that storing the samples at -20ºC in a bag that was filled with nitrogen gas and then evacuated can preserve fluorescence. Likewise, shipping the samples overseas requires similar conditions: nitrogen-filled, vacuumed, and cold. Additionally cutting section of 100 nm thickness instead of 70 nm preserved the fluorescence more reliably during the shipment. Extra caution needs to be paid during the summer when the samples can be exposed to very high temperatures.

STED imaging

For STED a solution of silica nanoparticles (Sicasta BlueF, 1 µm, NH_2 functionalized, Micromod GmbH Rostock) was diluted to 1/10000 with milliQ water. For LR White sections, about 10 µl of this solution were applied to each coverglass. For GMA sections the same silica nanoparticles were used, but diluted to 1/500. 10 µl of the solution were applied to each coverslip and washed off after 5 minutes of incubation. The samples were kept in nitrogen until the water had evaporated. All coverslips were mounted onto single concave microscope slides (SailingBoat Lab Co., Ningbo City, China), where the concave depression was filled with milliQ water. The samples were placed into a custom-designed STED microscope as previously described[27]. In brief, Citrine was excited at 490 nm by a diffraction-limited spot which was overlaid with a doughnut-shaped STED spot (at 590 nm) featuring zero intensity in the center. The STED spot prevents fluorescence by instantly driving excited molecules back to the ground state, except in proximity of the doughnut center. Therefore fluorescence is reduced to a volume smaller than the diffraction limit. For focusing we used high numerical aperture

objective lenses (1.4 NA PL APO, 100x, oil or 1.3 NA PL APO, 63x, glycerol, both Leica). The epifluorescence was filtered via a 525/60 band-pass filter and detected by an avalanche photodiode. The silica nanoparticles were excited at 405 nm and detected with a second detector channel at 450/60 nm. After STED imaging, the coverslips were removed from the microscope slides, dried, and sent back to Utah for electron microscopy.

PALM imaging

The gold nanoparticles solution (Micospheres-Nanospheres, 100 nm #790122-010 or 250 nm #790128-010) was diluted to 1/10 with milliQ water, which was filtered with a 0.22 μm syringe filter (Millipore, #SLGP033RB). The solution was applied to the coverslips, and after 4 minutes of incubation, the solution was washed off with the filtered milliQ water. The coverslips were placed in the coverslip holder for Zeiss PAL-M microscope (Carl Zeiss, PAL-M Prototype Serial No. 2701000005) equipped with a 100x plan-apochromat (NA=1.46) objective lens (Carl Zeiss, #420792-9800). The vacuum grease was applied on the rim of the coverslip holder to minimize the drift. The region of the interest was located in the bright field and then pre-bleached using the intensive 561 nm laser illumination (5 mW) for 2-5 minutes until the autofluorescence was quenched. 10,000-20,000 frames with a frame rate of 20-30/s were acquired using an Andor iXon DU-897D EMCCD camera (Andor Technology Plc) while photo-convertible 405 nm laser at 1-5 μW and read-out 561 nm lasers at 1-5 mW were applied simultaneously. The intensity of 405 nm laser was set so that it only activated a few molecules in each frame. The centroid of the molecules was calculated and mapped using Zeiss Zen PAL-M program (Carl Zeiss GmbH) with the drift correction applied. Localization precision was calculated using the equation:

$$\left\langle (\Delta x)^2 \right\rangle = \frac{\left(s^2 + a^2/12\right)}{N} + \frac{8\pi s^4 b^2}{a^2 N^2}$$

Where Δx is the error in localization, s is the standard deviation, N is the number of photons collected, a is the size of the pixel, and b is the background noise[21]. Generally, the brighter the signal, the better the localization because the brightest spot within a single fluorescent molecule can be refined to one pixel or only a few pixels in each fluorescence mass whereas a dark dim spot will have many more pixels with the same intensity. Thus knowing the center of the fluorescent molecule is more precise if the signal-to-noise ratio is better. On a cautionary note, one must keep in mind that each dot in the PALM image is not actually observed fluorescence but rather a calculated location of each fluorophore; because the dot size is controlled by the user, it is important not to set the dot size below the experimentally defined resolution. Background fluorescence leads to ambiguity in the protein localization but can be removed from the final image. Emission from fluorescent proteins such as tdEos and Dendra typically lasts for 500 ms or less whereas the emission from the background signals lasts longer than 500 ms. By selecting molecules that were fluorescent for less than 500 ms, most of the background fluorescence was removed.

SEM imaging

The sections on coverslips were stained for 4 minutes with 2.5% uranyl acetate in water to improve membrane contrast. The sections were carbon coated and then imaged

under high vacuum in a FEI Nova Nano scanning electron microscope. Backscattered electrons (BSE) were collected using a vCD detector. The immersion mode was applied to the field. The stage was negatively biased (the landing energy was set to 3 keV) to allow acceleration of backscattered electrons toward the detector. The accelerating voltage and the beam current were set at 5 keV and 0.11 nA, respectively. The grayscale of the image is then inverted to resemble TEM images, and thus, electron reflective structures appear black instead of white. The contrast was enhanced using Adobe Photoshop.

Alignment of fluorescence and electron micrographs

A fluorescence image and an electron micrograph of the same section were overlaid based on the silica bead or gold fiduciary markers, which appear electron dense in electron micrographs (**Supplementary Fig. 3a** and **Supplementary Fig. 4a**). First, the image of fiduciary markers was aligned on the micrographs using Adobe Photoshop (**Supplementary Fig. 3b** and **Supplementary Fig. 4b**). Autofluorescence from the tissue due to the UV illumination can be also used to refine the alignment. Based on the translation values we obtained from the fiduciary markers, the STED or PALM images were aligned to the corresponding electron micrographs (**Supplementary Fig. 3c** and **Supplementary Fig. 4c**). For liprin, the alignment could also be corrected at high magnification based on the perinuclear aggregation of Liprin in the electron micrograph and strong fluorescence from such aggregations in the fluorescent image. This was useful in the STED image since the beads sometimes moved and because the charging of the beads led to flare on the electron micrograph (**Supplementary Fig. 3a,b**).

For the merged panels, we applied a gradient transparency to the STED or PALM images using Adobe Photoshop so that the black background did not obscure the micrograph in the figures (**Supplementary Fig. 3d** and **Supplementary Fig. 4d**). The transparency of black pixels was set to 20%.

References:

1. Cox, G. & Sheppard, C.J. Practical limits of resolution in confocal and non-linear microscopy. *Microscopy Research and Technique* **63**, 18-22 (2004).
2. Hell, S.W. Far-field optical nanoscopy. *Science* **316**, 1153-1158 (2007).
3. Hell, S.W. & Wichmann, J. Breaking the diffraction resolution limit by stimulated emission: stimulated-emission-depletion fluorescence microscopy. *Opt. Lett.* **19**, 780-782 (1994).
4. Klar, T.A., Jakobs, S., Dyba, M., Egner, A. & Hell, S.W. Fluorescence microscopy with diffraction resolution barrier broken by stimulated emission. *Proc. Natl. Acad. Sci. U.S.A* **97**, 8206-8210 (2000).
5. Betzig, E. et al. Imaging Intracellular Fluorescent Proteins at Nanometer Resolution. *Science* **313**, 1642-1645 (2006).
6. Rust, M.J., Bates, M. & Zhuang, X. Sub-diffraction-limit imaging by stochastic optical reconstruction microscopy (STORM). *Nat. Methods* **3**, 793-795 (2006).
7. Hess, S.T., Girirajan, T.P.K. & Mason, M.D. Ultra-high resolution imaging by fluorescence photoactivation localization microscopy. *Biophys. J* **91**, 4258-4272 (2006).

8. Roth, J., Bendayan, M., Carlemalm, E., Villiger, W. & Garavito, M. Enhancement of structural preservation and immunocytochemical staining in low temperature embedded pancreatic tissue. *J. Histochem. Cytochem* **29**, 663-671 (1981).
9. Rostaing, P., Weimer, R.M., Jorgensen, E.M., Triller, A. & Bessereau, J. Preservation of immunoreactivity and fine structure of adult C. elegans tissues using high-pressure freezing. *J. Histochem. Cytochem* **52**, 1-12 (2004).
10. Morphew, M.K. 3D immunolocalization with plastic sections. *Methods Cell Biol* **79**, 493-513 (2007).
11. Murphy, R.M. et al. Size and structure of antigen-antibody complexes. Electron microscopy and light scattering studies. *Biophys. J* **54**, 45-56 (1988).
12. Sims, P.A. & Hardin, J.D. Fluorescence-integrated transmission electron microscopy images: integrating fluorescence microscopy with transmission electron microscopy. *Methods Mol. Biol* **369**, 291-308 (2007).
13. Micheva, K. & Smith, S. Array tomography: a new tool for imaging the molecular architecture and ultrastructure of neural circuits. *Neuron* **55**, 25-36 (2007).
14. Tsien, R. The green fluorescent protein. *Annual Review of Biochemistry* **67**, 509-544 (1998).
15. Mello, C.C., Kramer, J.M., Stinchcomb, D. & Ambros, V. Efficient gene transfer in C.elegans: extrachromosomal maintenance and integration of transforming sequences. *EMBO J* **10**, 3959-3970 (1991).
16. Frøkjaer-Jensen, C. et al. Single-copy insertion of transgenes in Caenorhabditis elegans. *Nat. Genet* **40**, 1375-1383 (2008).
17. Yeh, E., Kawano, T., Weimer, R.M., Bessereau, J. & Zhen, M. Identification of Genes Involved in Synaptogenesis Using a Fluorescent Active Zone Marker in Caenorhabditis elegans. *J. Neurosci.* **25**, 3833-3841 (2005).
18. Riemersma, J.C. Osmium tetroxide fixation of lipids for electron microscopy. A possible reaction mechanism. *Biochim. Biophys. Acta* **152**, 718-727 (1968).
19. Clancy, B. & Cauller, L.J. Reduction of background autofluorescence in brain sections following immersion in sodium borohydride. *J. Neurosci. Methods* **83**, 97-102 (1998).
20. Newman, G.R. & Hobot, J.A. *Resin Microscopy and On-Section Immuno-cytochemistry*. (Springer-verlag: Berlin, Germany, 1993).
21. Thompson, R. Precise Nanometer Localization Analysis for Individual Fluorescent Probes. *Biophysical Journal* **82**, 2775-2783 (2002).
22. Yguerabide, J. & Yguerabide, E.E. Light-Scattering Submicroscopic Particles as Highly Fluorescent Analogs and Their Use as Tracer Labels in Clinical and Biological Applications: II. Experimental Characterization. *Analytical Biochemistry* **262**, 157-176 (1998).
23. Joseph Goldstein et al. *Scanning Electron Microscopy and X-Ray Microanalysis*. (Springer Science + Business Media, LLS: New York, 2003).
24. Hell, S.W., Lindek, S., Cremer, C. & Stelzer, E.H.K. Measurement of the 4Pi-confocal point spread function proves 75 nm axial resolution. *Appl. Phys. Lett.* **64**, 1335 (1994).
25. Schmidt, R. et al. Mitochondrial Cristae Revealed with Focused Light. *Nano Letters* **9**, 2508-2510 (2009).
26. Shtengel, G. et al. Interferometric fluorescent super-resolution microscopy resolves

3D cellular ultrastructure. *Proceedings of the National Academy of Sciences* **106**, 3125-3130 (2009).
27. Punge, A. et al. 3D reconstruction of high-resolution STED microscope images. *Microsc. Res. Tech* **71**, 644-650 (2008).
28. Kanaji, S., Iwahashi, J., Kida, Y., Sakaguchi, M. & Mihara, K. Characterization of the Signal That Directs Tom20 to the Mitochondrial Outer Membrane. *J Cell Biol* **151**, 277-288 (2000).
29. Clark, S.G., Lu, X. & Horvitz, H.R. The Caenorhabditis Elegans Locus Lin-15, a Negative Regulator of a Tyrosine Kinase Signaling Pathway, Encodes Two Different Proteins. *Genetics* **137**, 987-997 (1994).
30. Weibull, C. & Christiansson, A. Extraction of proteins and membrane lipids during low temperature embedding of biological material for electron microscopy. *J Microsc* **142**, 79-86 (1986).

Supplementary File	Title
Supplementary Figure 1	Preservation of morphology and fluorescence by different fixatives
Supplementary Figure 2	Liprin localization at low magnification
Supplementary Figure 3	Silica beads were used to align fluorescence and electron micrographs
Supplementary Figure 4	Gold nanoparticles were used to align fluorescence and electron micrographs
Supplementary Figure 5	Histone localization in an intestinal nucleus is similar by correlative PALM-EM to what was observed using correlative STED-EM
Supplementary Table 1	Oligonucleotides
Supplementary Note 1	Strains
Supplementary Note 2	Choice of fluorescent proteins
Supplementary Note 3	Steps for sample preparation
Supplementary Note 4	Freezing and solvents
Supplementary Note 5	Components of each plastic

Figure 1, Watanabe et al.

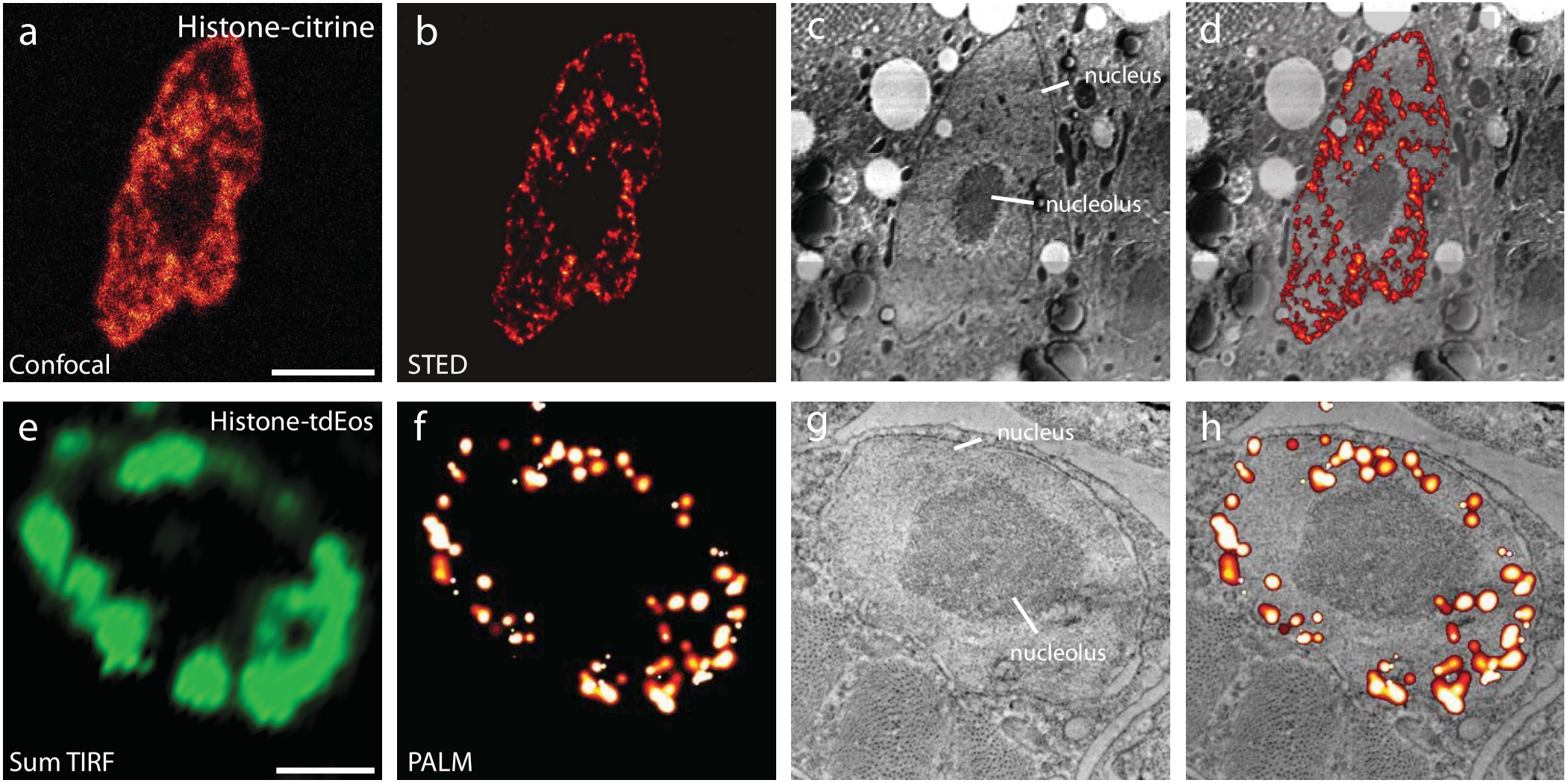

Figure 2, Watanabe et al.

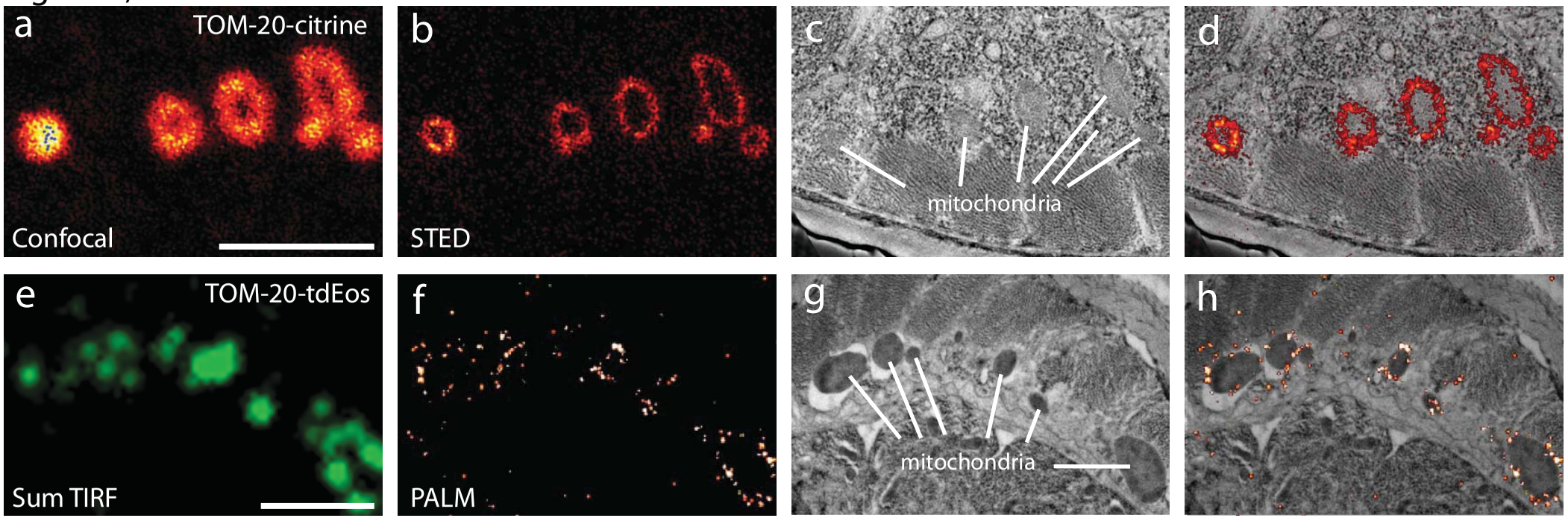

Figure 3, Watanabe et al.

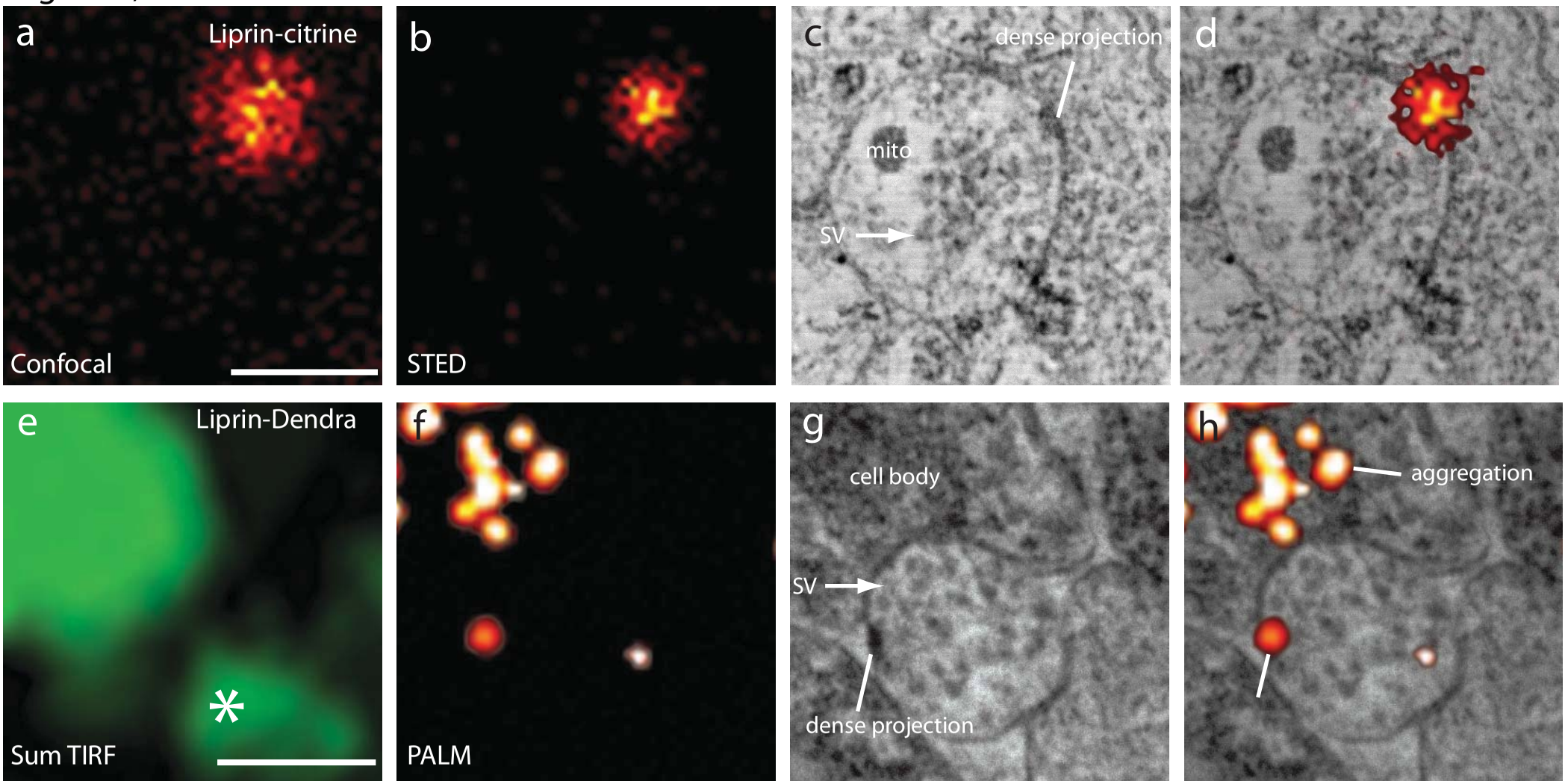

Supplementary Figure 1

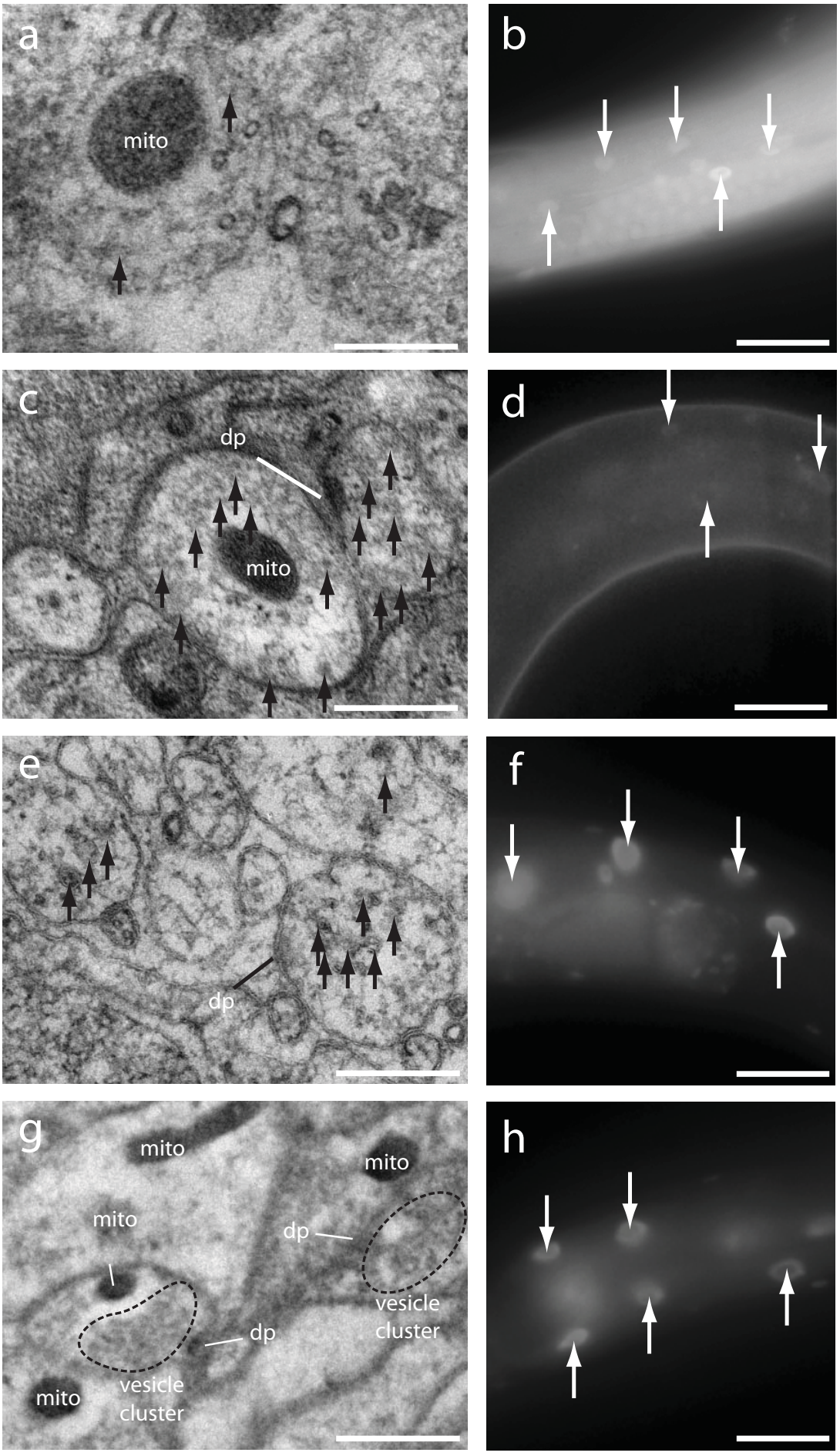

Supplementary Figure 1: Preservation of morphology and fluorescence by different fixatives. (**a**) A TEM image of ventral nerve cord (VNC) fixed with 1% glutaraldehyde. (**b**) fluorescence micrograph of intestinal nuclei fixed with 1% glutaraldehyde. (**c**) A TEM image of VNC fixed with 0.1% osmium tetroxide. (**d**) A fluorescence micrograph of intestinal nuclei fixed with 0.1% osmium tetroxide. (**e**) A TEM image of ventral nerve cord (VNC) fixed with 0.1% potassium permanganate. (**f**) A fluorescence micrograph of intestinal nuclei fixed with 0.1% potassium permanganate preserves fluorescence well. (**g**) TEM image of the nerve ring fixed with 0.1% potassium permanganate + 0.001% osmium tetroxide. (**h**) A fluorescence micrograph of intestinal nuclei fixed with 0.1% potassium permanganate + 0.001% osmium tetroxide. Fluorescence images were acquired prior to plastic polymerization. Electron micrographs were acquired using a TEM. Transgenic animals (Citrine-Histone) were used to obtain the fluorescence images (b, d, f, and h) and electron micrographs of (**e**) and (**g**). Transgenic animals (P*myo-2::GFP*) were used to obtain electron micrographs of (**a**) and (**c**). The gain and exposure time of the camera were the same for (**b**,**f**,**h**), but for (**d**), the gain was increased 4x, and the exposure time was increased from 430 ms to 1000 ms to visualize the signal. Arrowheads indicate fluorescent signals in nuclei. In all images, resin was LR White with 5% water, pH 6.5. Black arrowheads indicate each synaptic vesicle in the electron micrographs. 'mito', mitochondria; 'dp', dense projection. Scale bars, 300 nm (**a**,**c**,**e**,**g**) and 30 μm (**b**,**d**,**f**,**h**).

UU IR Author Manuscript

Supplementary Figure 2

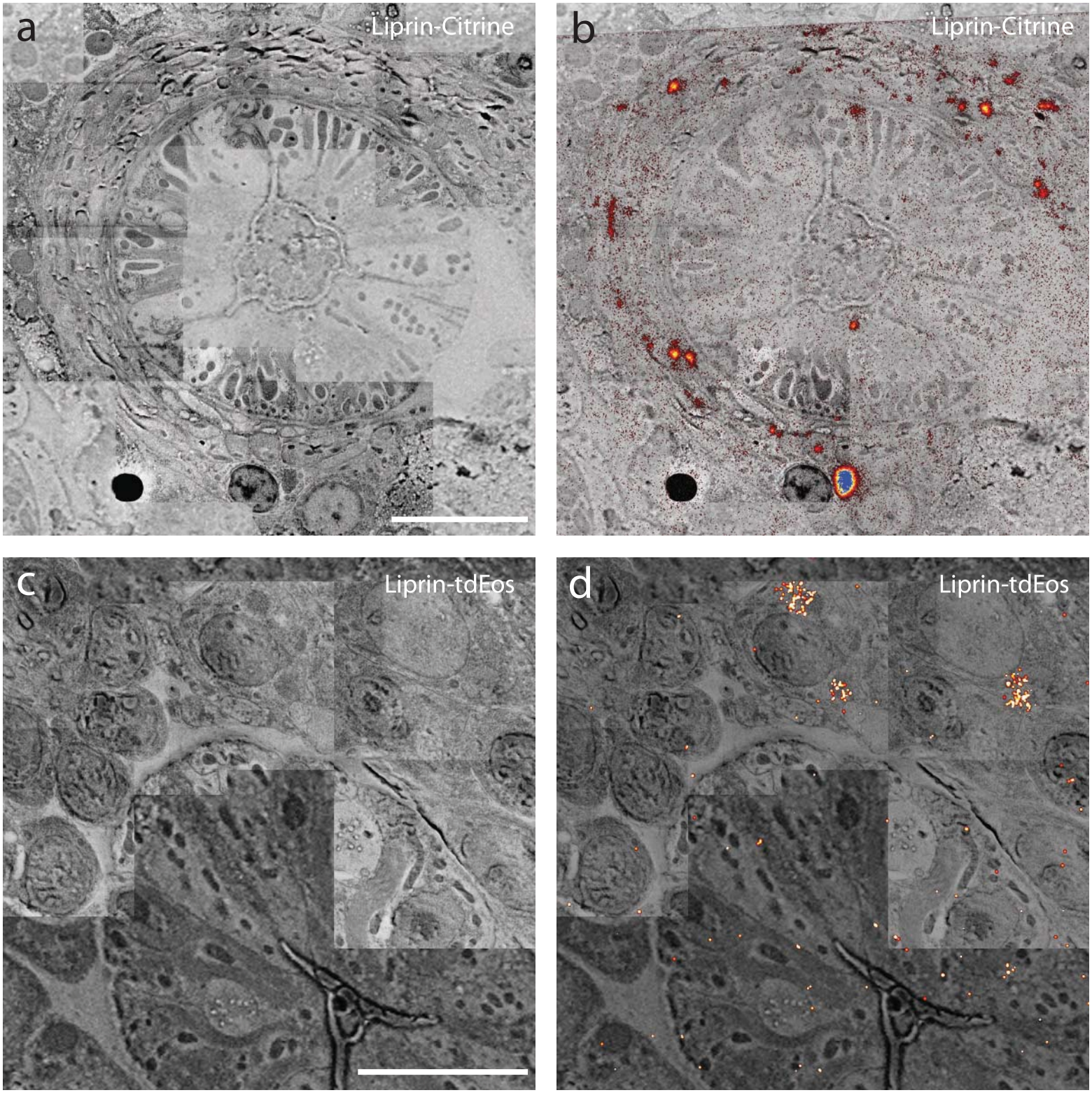

Supplementary Figure 2: Liprin localization at low magnification. High magnification electron micrographs of neurons are tiled on top of low magnification micrographs to depict morphology and protein localization in the nerve ring and head ganglia. (**a**) Electron micrograph of nerve ring of a Liprin-Citrine expressing strain, (**b**) Correlative STED and electron micrograph of Liprin-Citrine. Note large aggregate of liprin adjacent to the nucleus of a neuron cell body at the bottom of the micrograph. (**c**) Electron micrograph of head ganglion. (**d**) Correlative PALM and electron micrograph of Liprin-Dendra. Note the aggregations of liprin in the cell bodies adjacent to the nuclei. Scale bars, 5 μm (**a**-**d**).

UU IR Author Manuscript

Supplementary Figure 3

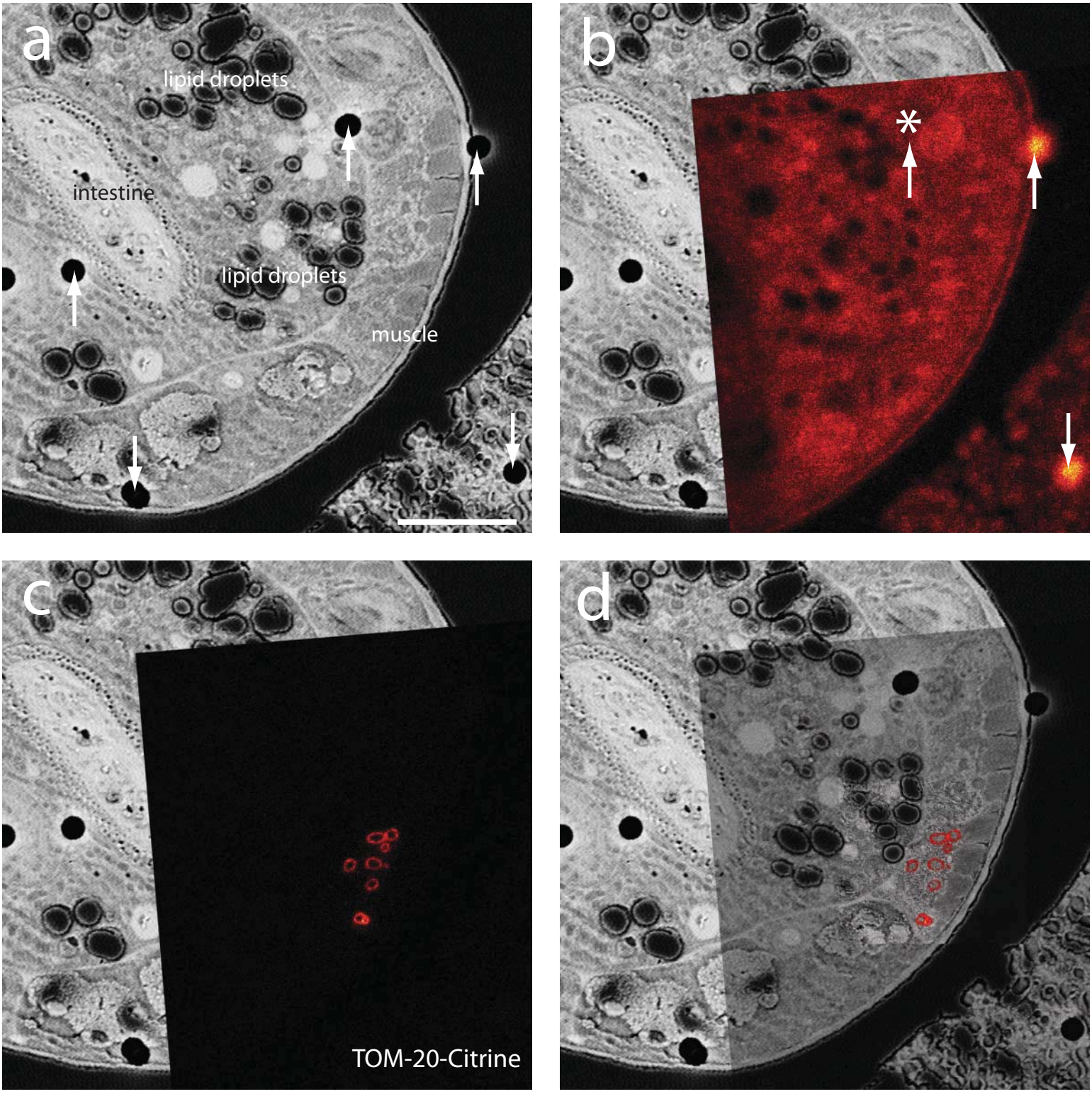

Supplementary Figure 3: Silica beads were used to align fluorescence and electron micrographs. (**a**) A low magnification electron micrograph (5000x) from a cross section of *C. elegans* expressing TOM-20-Citrine. Black circles, indicated by white arrowheads, are the fiduciary marks from silica beads applied prior to STED imaging. (**b**) An image of fiduciary markers is aligned onto an electron micrograph based on the location of the fiduciary marks. * indicates a silica bead that was not present during the STED recording. Presumably the bead moved during the post-staining with uranyl acetate just prior to SEM imaging. (**c**) The STED image is then rotated and translated based on the values obtained in (**b**). (**d**) A gradient transparency is applied to the STED image so that the transparency of the background is reduced to 20% while that of citrine fluorescence remains at 100%. Scale bars, 5 μm (**a**-**d**).

UU IR Author Manuscript

Supplementary Figure 4

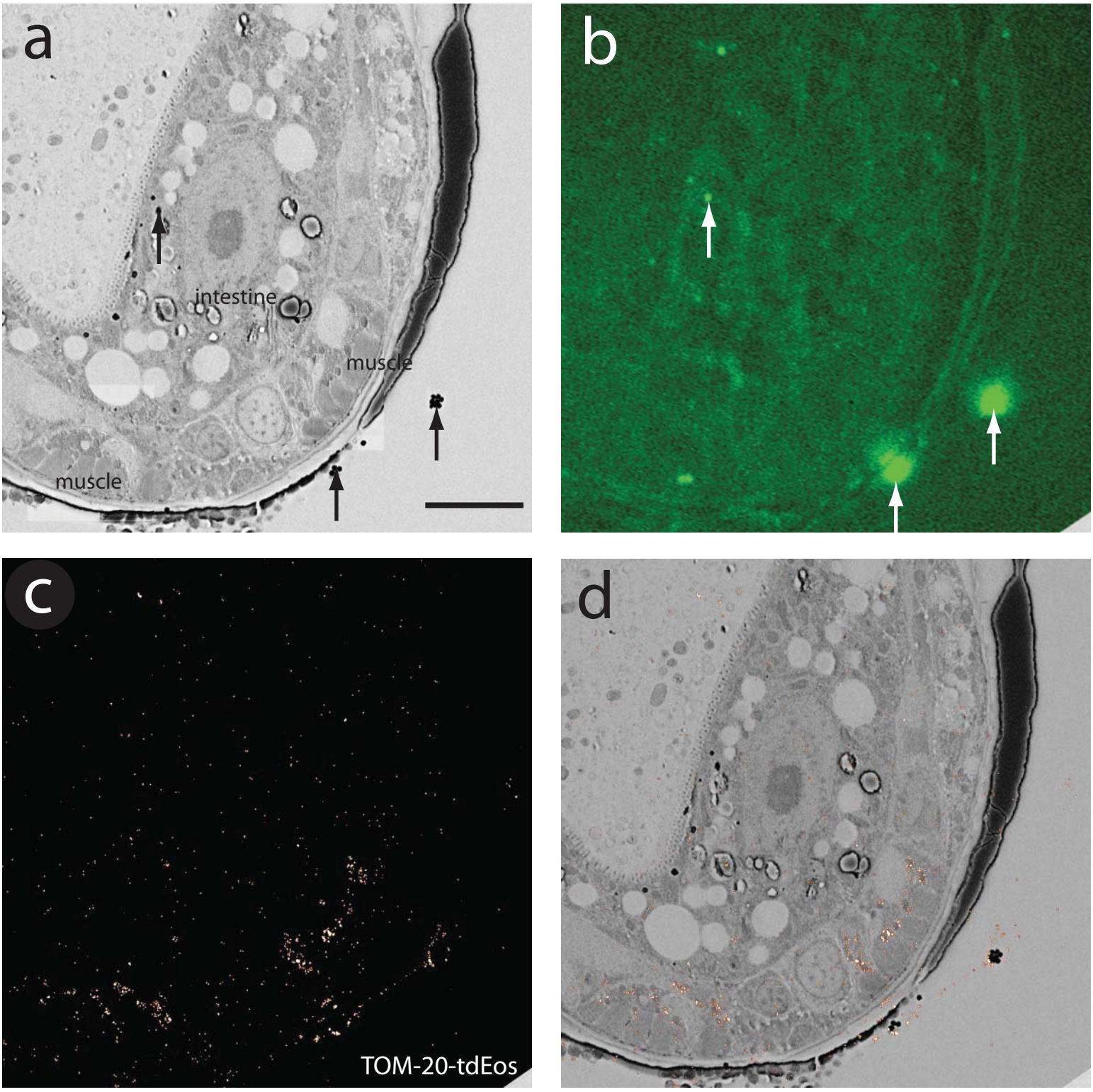

Supplementary Figure 4: Gold nanoparticles were used to align fluorescence and electron micrographs. (**a**) A low magnification electron micrograph from a cross section of *C. elegans* expressing TOM-20::tdEos. Black dots are the fiduciary marks from 100 nm gold nanoparticles applied prior to PALM imaging. (**b**) An image of fiduciary markers is aligned onto an electron micrograph based on the location of the fiduciary marks. Note that the two bright spots on the lower right arise from clusters of gold particles. (**c**) A PALM image is then rotated and translated based on the values obtained in (**b**). (**d**) A gradient transparency is applied to the PALM image so that the transparency of the background is reduced to 20% while that of tdEos fluorescence remains at 100%. Scale bars, 5 μm (**a**-**d**).

UU IR Author Manuscript

Supplementary Figure 5

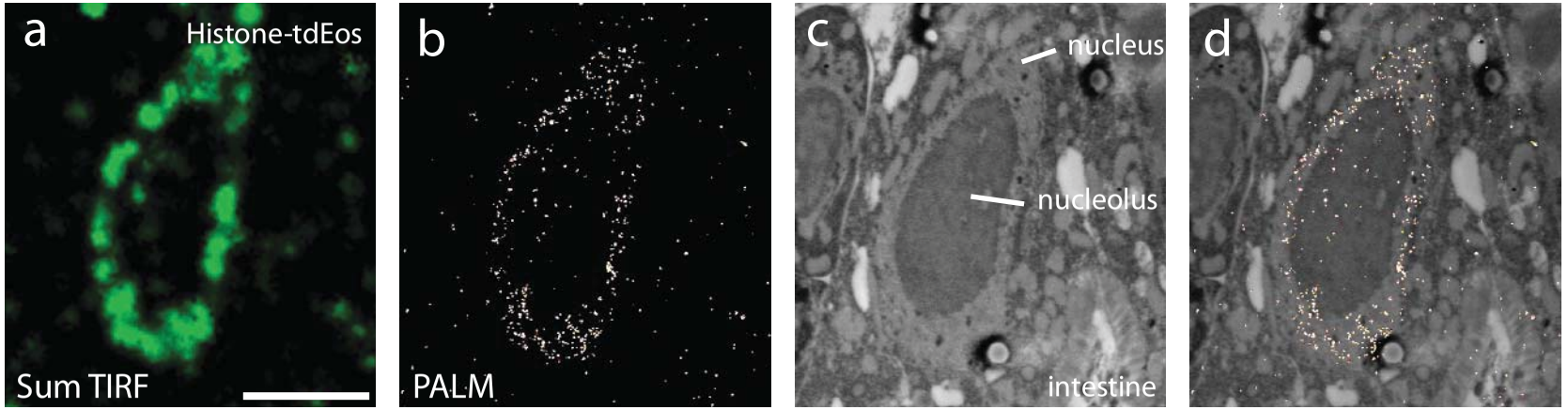

Supplementary Figure 5: Histone localization in an intestinal nucleus is similar by correlative PALM-EM to what was observed using correlative STED-EM. (**a**) Sum TIRF image of Histone-tdEos acquired from a thin section (70 nm). Sum TIRF image represents all the photons detected by the camera during the experimental time course. (**b**) Corresponding PALM image of Histone-tdEos. (**c**) Electron micrograph of an intestinal cell nucleus acquired from the same section. (**d**) Correlative PALM and electron microscopy of Histone-tdEos. The fluorescent signals are tightly localized to the nucleus. The sample was embedded in LR White. Scale bars, 3 μm (**a**-**d**).

UU IR Author Manuscript

Supplementary Table 1: Oligonucleotides

oGH55	GGGACAAGTTTGTACAAAAAAGCAGGCTTAAAAATGAGTAAAGGAGAAGAACTTTTCACT
oMPD6	GGGGACCACTTTGTACAAGAAAGCTGGGTATTTGTATAGTTCATCCATGCC
oGH95	GGGGACAAGTTTGTACAAAAAAGCAGGCTTCGCCACCATGAGTGCGATTA
EOS_rev	GGGGACCACTTTGTACAAGAAAGCTGGGTgTCGTCTGGCATTGTCAGGCAATC
oGH76	TCTTGTACAAAGTGGTGAGTAAAGGAGAAGAACTTTTCACTG
oGH57	TGGCGTCGATCATCCTTTGTATAGTTCATCCATGCC
oGH96	TCTTGTACAAAGTGGTCGCCACCATGAGTGCG
oGH94	TGGCGTCGATCATCCTGGCTGATTATGATCTAGAGTCGCG
oGH38	CCACTTTGTACAAGAAAGTTGAAC
oGH39	GGATGATCGACGCCAAC
oRJH19	GGGGACAAGTTTGTACAAAAAAGCAGGCTGTTATTCACTTTCTGCAAGGTATGAC
oRJH20	GGGGACCACTTTGTACAAGAAAGCTGGGTAGGTATATAAATGAAACTCGTAGGATTTTGC
oRJH21	tggagggatccATGAACACCCCGGGAATTAACC
oRJH22	tgctaactagtGTTGGAATTCGAAGCTTGAGCTC
oRJH23	GGGGACAACTTTGTATAGAAAAGTTGTTCCTTCAGAAGACGTGCTTTCC
oRJH24	GGGGACTGCTTTTTTGTACAAACTTGGGTGACTGAAAGTTTGATTG

UU IR Author Manuscript

Supplementary Note 1: Strains
The wild type is Bristol N2.
EG5582 *oxSi282*[P*hsp-16.41::Citrine::HIS-11::unc-54 3'UTR*] II; *unc-119(ed3)* III
EG5576 *oxSi283*[P*hsp-16.41:: tdEos::HIS-11::unc-54 3'UTR*] II ; *unc-119(ed3)* III.
EG5515 *lin-15(n765ts)* X ; *oxEx1329* [P*myo-3::TOM-20(N-term)::Citrine::let-858 3'UTR lin-15(+)* LITMUS 38i]
EG5998 *oxSi203* [P*myo-3::TOM-20(N-term)::tdEos::let-858 3'UTR unc-119(+)*] II ; *unc-119(ed3)* III
EG6190 *ttTi5605; unc-119; oxEx1490*[P*snt-1::SYD-2::citrine*; *unc-119(+) lin-15(+)*]
EG6191 *ttTi4348; unc-119; oxEx1491*[P*snt-1*::*SYD-2::Dendra2*; *unc-119(+) lin-15(+)*]

Supplementary Note 2: Choice of fluorescent proteins
For STED microscopy, fluorescent proteins must possess a high photostability. eYFP and Citrine have been shown to be well-suited for STED[1]. We choose Citrine as the fluorophore for STED because the quantum yield is slightly higher, and the transgenes (Citrine-Histone, TOM-20-Citrine, and liprin-Citrine) were expressed well in *C. elegans* animals.

For PALM, the fluorescent protein must be capable of conversion from a fluorescence inhibited (inactivated) to a non-inhibited (activated) state. Here, we focused on photo-convertible rather than simply photo-activatable fluorescent proteins since the preservation of fluorescence can be visualized and assessed before photoconversion. For example, Dendra and EosFP emit green light before photo-conversion, and red light after photo-conversion.

We evaluated potential photo-convertible fluorescent proteins based on the following characteristics: appropriate expression pattern in *C. elegans*, high photo-conversion efficiency, and bright fluorescence after photo-conversion. We examined mOrange, Dendra, mEosFP, mEosFP2, and tdEos for reliable expression in *C. elegans*. Fusion of mEosFP2 to TOM-20 caused perinuclear aggregations of the fluorescence in muscle cells, suggesting that the tag was causing proteins to aggregate. mOrange, Dendra, mEosFP, and tdEos fusions to TOM-20 appeared to be expressed in the expected locations in the cell.

Genes for different fluorescent proteins were fused to the open reading frame for histone H2B under the control of the heatshock promoter. The constructs were inserted into the genome using *Mos1*-mediated single copy insertion (MosSCI)[2]. Following a heat shock, the photo-conversion of each fluorophore was tested in whole animals by exposing them to 405 nm light (or 488 nm for mOrange[3]). Only mOrange was not detectably photo-converted. The transgenic strains expressing Dendra, mEosFP, or tdEos were fixed using 0.1% potassium permanganate and embedded in LR White. We prepared 100 nm slices from each and compared the photon intensity after the photo-conversion on a Zeiss PAL-M microscope.

Supplementary Note 3: Steps for sample preparation
The sample preparation for electron microscopy consists of six steps. Rapid freezing under high pressure immobilizes water molecules without generating ice crystals[4]. The vitreous water is then replaced by a fixative dissolved in organic solvents such as acetone. Fixation of rapidly frozen tissue can preserve morphology better than

conventional fixation in which cells are immersed in fixatives. Plastic resin is then infiltrated into the fixed and dehydrated tissues and polymerized into a plastic block. Finally, the hardened block is sliced into ultra-thin sections of 30-70 nm and mounted. Each of these steps could potentially quench fluorophores and had to be optimized.

Supplementary Note 4: Freezing and solvents

To determine if freezing under high pressure reduced fluorescence, we simply froze animals expressing GFP in the pharyngeal muscles (*Pmyo-2::GFP*) and thawed them to room temperature without any further treatment. The fluorescence level in the frozen animals was comparable to animals that were not frozen. By contrast, organic solvents quenched fluorescence. The same transgenic strain was frozen and processed through the freeze-substitution either with 100% acetone or 95% acetone plus 5% water in the absence of fixatives. The fluorescence in the animals treated with 100% acetone was completely quenched while there was no reduction in fluorescence in animals processed with 95% acetone, compared with non-treated animals. The presence of water at all steps was essential for the maintenance of fluorescence[5]. Each of the remaining steps also perturbs fluorescence significantly; to maintain fluorescence signals certain fluorescent proteins, fixatives and resins were required.

Supplementary Note 4: Components of each plastic

Lowicryl K4M is a combination of triethyleneglycol-di-methacrylate and benzoin-methyl-ether with acrylic and methacrylic esters.

LR Gold is consisted of 80% Polyhydroxy substituted bisphenol A dimethacrylate resin, 19.6% C12 methacrylate ester, and 0.4% dimethyl para toluidine.

LR White is consisted of 80% Polyhydroxy substituted bisphenol A dimethacrylate resin,19.6% C12 methacrylate ester, and 0.9% benzoyl peroxide.

References for Supplemenary Notes

1. Nägerl, U.V., Willig, K.I., Hein, B., Hell, S.W. & Bonhoeffer, T. Live-cell imaging of dendritic spines by STED microscopy. *Proc. Natl. Acad. Sci. U.S.A* **105**, 18982-18987 (2008).
2. Frøkjaer-Jensen, C. et al. Single-copy insertion of transgenes in Caenorhabditis elegans. *Nat. Genet* **40**, 1375-1383 (2008).
3. Kremers, G., Hazelwood, K.L., Murphy, C.S., Davidson, M.W. & Piston, D.W. Photoconversion in orange and red fluorescent proteins. *Nat Methods* **6**, 355-358 (2009).
4. McDonald, K. Cryopreparation methods for electron microscopy of selected model systems. *Methods Cell Biol* **79**, 23-56 (2007).
5. Micheva, K. & Smith, S. Array tomography: a new tool for imaging the molecular architecture and ultrastructure of neural circuits. *Neuron* **55**, 25-36 (2007).